Novel Fuzzy-Based Open-Switch Fault Detection Scheme of Voltage Source Inverter Induction Motor Drive

Ahmed S. Gardouh, Sayed Abulanwar, *Senior Member, IEEE*, Fujin Deng, *Senior Member, IEEE*, Eid Gouda, and Abdelhady Ghanem, *Member, IEEE*

***Abstract*—This article proposes a novel real-time fault diagnosis approach for open-switch faults of three-phase pulsewidth modulated voltage source inverter induction motor drive system. The diagnosis method relies only on the observed current via processing the extracted dc components and current absolutes using dynamic resonant filters (DRFs). By employing the ratio between the extracted dc components along with the dc component of absolute line currents and absolute line currents sum, 33 different types of faults can be detected and discriminated effectively. A fuzzy logic-based subsystem is dedicated to accurate reporting of different fault scenarios and manipulating the detection delay caused by the extracted dc component oscillation introduced by the DRFs. The proposed approach is parameter-free, fast, reluctant to noise presence, applicable for a wide range of switching frequencies, and independent of load-level or transient variations. Besides, it is suitable for any type of control technique either open or closed loop without any excessive sensors. Extensive experimental and time-domain investigations are examined, and the obtained results reveal the effectiveness of the proposed fault detection method.**

***Index Terms*—Current-sensor fault, fault detection, fault diagnosis, induction motor (IM), open-switch fault, voltage source inverter (VSI).**

I. Introduction

THE three-phase induction motor (IM) is a pivotal hinge of industrial applications due to its reliability, robust structure, self-starting, and low maintenance cost [1]. Virtually, IM drive systems are dictated by pulsewidth modulated voltage source inverter (PWM-VSI) with fixed dc voltage. Various control structures can be implemented to manipulate PWM-VSI to realize direct and independent control of the machine flux and torque [2]. The aforesaid setup is usually prone to overloading and/or harsh environmental conditions that might lead to internal or voltage source inverter (VSI) open-switch faults [3].

It is reported that IM drive system failures are attributed to VSI (38%), control circuits (53.l%), and external auxiliaries (7.l%), respectively [4]. Power circuit faults in VSI can be categorized into short-circuit and open-circuit faults. Being characterized by a higher fault current, short-circuit faults can be effectively mitigated by protection schemes [5]. Yet, the detection of open-switch faults is onerous and the IM drive system might run for a long time yielding thermal stresses on the other healthy switches that can cause cascaded faults. In addition, open-switch faults result in excessive torque ripples of the motor shaft [5], [6]. Hence, prompt detection of open-switch faults is crucial to avoid the aforementioned issues.

In the literature, various techniques for identifying open-switch faults can be categorized into model-based [7], [8], [9], [10], [11], [12], voltage-based [13], [14], [15], [16], and current-based techniques [17], [18], [19], [20], [21], [22], [23], [24], [25], [26], [27]. Besides, knowledge-based approaches have recently gained marked interest to be embedded with the abovementioned techniques [28], [29], [30], [31]. Model-based methods involve the selection of an appropriate model and the choice of a suitable observer. In [7], a proposed method for sensorless vector control utilizing the voltage error of a voltage-current hybrid model flux observer. In [8], the identification of open-switch faults is realized by employing the amplitude and phase characteristics of the residual vector, which represents the difference between the currents estimated by the observer and the measured currents. However, the aforesaid two approaches are effective only for detecting single open-switch faults. A fault diagnosis approach leveraging the mean values of current residuals during a fundamental period between the measured current and the current estimated by an observer, along with an adaptive threshold is proposed in [9]. Wang et al. [10] introduced a method for estimating the relative β-axis residual voltage. This estimation is achieved through the comparison of the reference voltage, determined using the switch duty cycle signal, with the output voltage estimated by a healthy machine model. The resulting

Manuscript received 21 March 2024; revised 2 July 2024; accepted 28 July 2024. Date of publication 6 August 2024; date of current version 11 September 2024. This work was supported in part by the National Key Research and Development Program of China under Grant 2022YFE0196300 and in part by the Science, Technology & Innovation Funding Authority (STDF) under Grant 46505. Recommended for publication by Associate Editor D. G. Xu. *(Corresponding author: Fujin Deng.)*

Ahmed S. Gardouh, Eid Gouda, and Abdelhady Ghanem are with the Electrical Engineering Department, Faculty of Engineering, Mansoura University, Mansoura 35516, Egypt (e-mail: ahmed_samir@mans.edu.eg; eaidgoda@mans.edu.eg; aghanem_m@mans.edu.eg).

Sayed Abulanwar is with the Electrical Engineering Department, Faculty of Engineering, Mansoura University, Mansoura 35516, Egypt, and also with the Faculty of Engineering, Horus University-Egypt, New Damietta 34518, Egypt (e-mail: abulanwar@mans.edu.eg).

Fujin Deng is with the Jiangsu Key Laboratory of Smart Grid Technology and Equipment, and the School of Electrical Engineering, Southeast University, Nanjing 210096, China (e-mail: fdeng@seu.edu.cn).

Color versions of one or more figures in this article are available at https://doi.org/10.1109/TPEL.2024.3438989.

Digital Object Identifier 10.1109/TPEL.2024.3438989

voltage residuals serve as fault indicators, with their polarities utilized for fault location. While this method demonstrates robustness against transient conditions and parameter changes, it is limited to the detection of single open-switch faults. Shu et al. proposed a fault diagnosis technique for model predictive control systems. This method leverages an inverter model to estimate the output phase voltage, enabling the identification and diagnosis of 18 open-switch fault cases [11]. In [12], the difference between the estimated and actual currents, determined by a differential current observer, is used to calculate residuals. Changing the polarity of the voltage reference alters the polarity of both the current and the residuals. Hence, open-switch faults can be identified by analyzing the variation in the residuals with an adaptive threshold. Generally speaking, model-based methods are inherently limited by the accuracy of the system model, parameter sensitivity, and designated thresholds, thus worsening the diagnostic performance.

Approaches relying on voltage for quick fault diagnosis are researched in [13], [14], [15], and [16]. While these methods achieve an adequate performance with rapid detection, they are usually associated with additional voltage sensors and/or other auxiliary circuits. The evaluation of PWM and line-to-line voltage levels during switching intervals using two voltage sensors and an additional circuit for identifying single and multiple open switches is suggested in [13]. Nevertheless, open-phase faults are not considered. An efficacious technique devoted to detecting single open-switch faults counting on the envelope of the output line-to-line voltage is presented in [14]. In [15], two line voltages are allocated as markers for detecting single and multiple open-switch faults. The faulty phase is identified by observing the ratio of magnitudes of these two signals while identifying the faulty switch is executed by examining their difference. Although this method can promptly detect faults within $1/20$ to a half-cycle, it requires a high computational burden due to the higher sampling rate. Open-switch faults are detected relying on the output phase voltages using a sliding window counting criterion. Post-fault, the affected phase voltage profile dramatically falls during specific half periods, allowing a robust indicator for an open-switch fault in [16].

On the contrary, current-based methods avert the need for additional sensors, thereby decreasing both costs and system complexity. The reconstruction of the $\alpha\beta$ current trajectories through elliptical fittings is presented in [17]. It leverages the disparities between elliptical axes and center coordinates to detect open-switch faults within less than half a cycle showcasing resilience against transient dynamics. However, it is essential to note that this approach solely addresses single open-switch faults. In [18], the current signals are subjected to windowing and seasonal-trend decomposition. Two indexes are devised for the seasonal and trend components, employing two thresholds for each to detect and locate nine open-switch fault cases within 1.3 current fundamental cycles with a high computational burden. In [19], the three-phase currents correlation using covariance is analyzed, and a sliding window spanning cycle is proposed for the identification of single open-switch or open-phase faults. The identification of single open-switch faults via the trajectory of phase currents is examined in [20]. Single and double open-switch faults are discriminated in [21] through the analysis of slope changes in adjacent trend lines within the $\alpha\beta$ reference frame of the current vector trajectory. In contrast to the previous method that relies on the trajectory of phase currents, this technique can pinpoint more faults but increases computation requisites. Moreover, in [22], the phase currents information, along with the average current Park's vector and fuzzy logic approach, is applied to process the fault variables and detect faulty open switches. The approach in [24] analyzes the phase current waveforms in real time, extracting abnormal patterns incurred by open-switch faults to identify various fault classes. A double normalization-based technique encompassing both current and angle normalization is proposed in [25] for detecting open-circuit faults. The normalized dc components extracted from the $\alpha\beta$ currents to diagnose open-switch faults are investigated in [26]. However, this method fails to detect two concurrent upper or lower open-switch faults. In [27], an online open-switch fault detection scheme based on sampled motor stator current manipulated by Padé approximation formula is presented. The latter extracts the inherently existing dc current component caused by the open-circuit fault. However, a high computational burden is requested to store at least 40 samples of the current with limited capacity to identify various fault types.

knowledge-based methods dispense with mathematical models, but entail significant training and excessive computational effort to achieve the satisfactory performance. Also, the knowledge-based methods encounter pronounced limitations in discriminating new scenarios that are not involved within their knowledge domains. A deep learning AI-based technique employing a blend of features for accurately pinpointing open-switch faults is introduced in [28]. For this, the suggested technique extracts 10 distinct signal features from each current signal, with 30 net signal features from each data set. A system that integrates a model-based diagnostic approach with a machine learning technique is introduced in [29]. In [30], the identification of faults involves extracting time-domain features from output voltage, output current, and input current, followed by employing the random forest and K-nearest neighbor methods

This article provides a novel current-based fault detection scheme for VSI fed IM. The central premise of the suggested technique is extracting the dc components of three line currents, their absolute, and the absolute of the three currents' summation. The major contributions of this article can be listed as follows.

1) Unlike several techniques, the proposed approach can effectively identify 33 types of open-circuit faults including variety of open-switch faults in the same or different legs and also current-sensor failures without any extra hardware and irrespective of the employed switching control strategy.
2) The proposed approach is simple and intuitive as the extraction of the dc components is achieved through the utilization of dynamic resonant filters (DRFs).
3) The proposed approach is entirely independent of motor parameters, motor rating, or loading condition. Besides, provides high accuracy even in the presence of signal noise and for a wide range of switching frequencies.

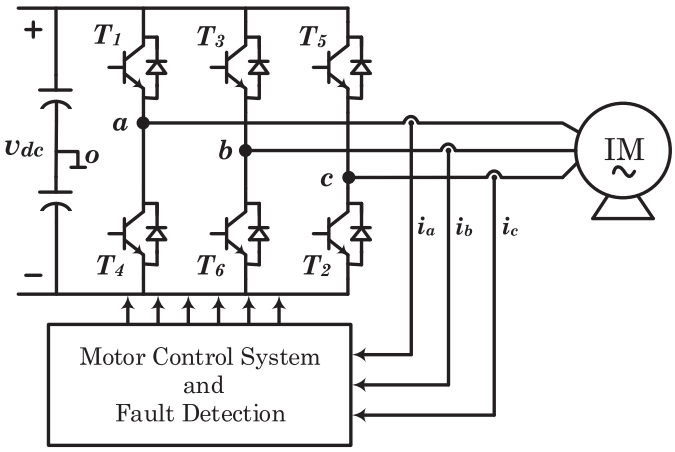

Fig. 1. Two-level VSI IM drive system.

4) Rapid and accurate reporting of all faults is guaranteed in favor of employing a fuzzy-based subsystem, which mitigates the effect of extracted dc component oscillation introduced by the DRFs.

II. System Description and Fault Type Analysis

Fig. 1 illustrates a schematic of a two-level VSI driving a three-phase IM. The motor control employs voltage/frequency (V/f) control technique with the motor line currents being monitored to achieve the rewarded flux and torque control.

The VSI comprises three parallel legs, fed by a dc link of constant dc voltage typically supplied by a rectifier and capacitor bank. Each leg is constructed with two semiconductor switches $(T_i, T_{i+3},\ \ i = 1, 2, 3)$ accompanied by antiparallel freewheeling diodes (D_i, D_{i+3}) to allow a negative current path across the switch. During normal operation, the line currents are represented by

$$\begin{cases} i_a = I_m \sin(\omega t) \\ i_b = I_m \sin(\omega t - \frac{2\pi}{3}) \\ i_c = I_m \sin(\omega t + \frac{2\pi}{3}). \end{cases} \tag{1}$$

I_m is the amplitude of line currents and ω is the angular frequency.

Away from open-leg faults, upon the occurrence of an open-switch fault, the ratio of the dc component of the faulty phase current to that of its corresponding absolute value is ± 1 depending on whether the faulty switch is upper or lower. Conversely, this ratio is $\ll 1$ in the other unaffected phases. In addition, in cases of open-leg or current-sensor faults, the measured current value of the affected phase or faulty sensor is zero. Consequently, it is reasonable to assert that the dc component of the absolute value of this current is also zero. Leveraging these distinctive features enables the differentiation between various types of open-switch faults. The proposed fault detection scheme can detect 33 different fault cases including open-switch faults as well as current-sensor failures. The analysis of the various fault scenarios is discussed in the following sections.

A. Single Open-Switch Fault

Upon occurrence of an open switch, the respective line current undergoes loss of either the positive or negative half-cycle, based on the faulty switch. For instance, faulty T_1 results in the loss of i_a in the positive half-cycle. The analysis of current asymmetry in steady-state is conducted using a Fourier series. In this regard, the three line currents are formulated as [32]

$$\begin{cases} i_a = -|i_a| = I_m \sin(\omega t) - \frac{I_m}{2}\sin(\omega t) - I_{\text{dc}} + \Delta i_a \\ i_b = I_m \sin(\omega t - \frac{2\pi}{3}) + \frac{I_m}{4}\sin(\omega t) + \frac{I_{\text{dc}}}{2} - \frac{\Delta i_a}{2} \\ i_c = I_m \sin(\omega t + \frac{2\pi}{3}) + \frac{I_m}{4}\sin(\omega t) + \frac{I_{\text{dc}}}{2} - \frac{\Delta i_a}{2} \end{cases} \tag{2}$$

$$I_{\text{dc}} = \frac{I_m}{\pi} = 0.3183 I_m \tag{3}$$

$$\Delta i_a = \sum_{n=1,2,\ldots} \frac{2I_m}{\pi(4n^2-1)} \cos(2n\omega t). \tag{4}$$

I_{dc} is the dc current component and Δi_a represents the oscillatory component of the current. Depending on the faulty switch, the dc component value of the three line currents varies from zero to either a positive or negative value. If the faulty switch is located in phase b or phase c the same analysis is carried out.

Accordingly, when the faulty switch is T_6, the phase b current can be expressed as

$$i_b = |i_b| = I_m \sin\left(\omega t - \frac{2\pi}{3}\right) - \frac{I_m}{2}\sin\left(\omega t - \frac{2\pi}{3}\right) + I_{\text{dc}} - \Delta i_b. \tag{5}$$

Similarly, when T_2 is faulted, phase c current, i_c, can be derived as

$$i_c = |i_c| = I_m \sin\left(\omega t + \frac{2\pi}{3}\right) - \frac{I_m}{2}\sin\left(\omega t + \frac{2\pi}{3}\right) + I_{\text{dc}} - \Delta i_c \tag{6}$$

where Δi_b and Δi_c signify the oscillatory components of the currents i_b and i_c, defined as

$$\Delta i_b = \sum_{n=1,2,\ldots} \frac{2I_m}{\pi(4n^2-1)} \cos\left(2n\omega t - \frac{4n\pi}{3}\right) \tag{7}$$

$$\Delta i_c = \sum_{n=1,2,\ldots} \frac{2I_m}{\pi(4n^2-1)} \cos\left(2n\omega t + \frac{4n\pi}{3}\right). \tag{8}$$

B. Two Open-Switch Fault in Different Legs, Upper, and Lower Switches

In this case, two out of the three line currents encounter loss of either the positive or negative half-cycle according to the faulty switch. Referring to loss of conduction of both T_5 and T_4, i_a will no longer include its negative half-cycle, while i_c loses its positive half-cycle. Accordingly, the line currents can be described as

$$\begin{cases} i_a = |i_a| = \frac{I_m}{2}\sin(\omega t) + I_{\text{dc}} - \Delta i_a \\ i_b = \frac{I_m}{2}\sin(\omega t - \frac{2\pi}{3}) + \Delta i_a - \Delta i_c \\ i_c = -|i_c| = I_m \sin(\omega t + \frac{2\pi}{3}) - I_{\text{dc}} + \Delta i_c. \end{cases} \tag{9}$$

C. Two Open-Switch Fault, Both Upper or Lower

The analysis of this case shows that the three line currents lose their positive or negative half-cycle in response to the faulty switches. In response to faulty T_6 and T_2, both i_b and i_c suffer loss of their negative half-cycles. Hence, the positive half-cycle of i_a is absent owing to the conduction dependency of T_1 on T_6 and T_2. Notably, this fault type will always coincide with three open-switch fault (i.e., two upper or lower switches in two different legs and the other at the opposite position in the third leg). In this context, the three-phase line currents can be derived as

$$\begin{cases} i_a = -|i_a| = \frac{I_m}{2}\sin(\omega t) - 2I_{\text{dc}} + \Delta i_b + \Delta i_c \\ i_b = |i_b| = \frac{I_m}{2}\sin(\omega t - \frac{2\pi}{3}) + I_{\text{dc}} - \Delta i_b \\ i_c = |i_c| = \frac{I_m}{2}\sin(\omega t + \frac{2\pi}{3}) + I_{\text{dc}} - \Delta i_c. \end{cases} \tag{10}$$

D. Open-Phase Faults

This fault signifies to two open switches in the same leg. Therefore, one of the three line currents will be zero based on the faulty switches. For instance, upon loss of the switches T_1 and T_4 of the leg of phase a, i_a will be zero and the line currents can be given as

$$\begin{cases} i_a = |i_a| = 0 \\ i_b = \sqrt{3}I_m[\sin(\omega t - \frac{2\pi}{3}) + \frac{1}{2}\sin(\omega t)] \\ i_c = \sqrt{3}I_m[\sin(\omega t + \frac{2\pi}{3}) + \frac{1}{2}\sin(\omega t)] \end{cases} \tag{11}$$

$$i_a + i_b + i_c = 0. \tag{12}$$

E. Three Open-Switch Fault Including Two Switches in the Same Leg

In this fault type, one of the three line currents will be zero and other currents will lose their positive or negative half-cycle based on the faulty switches. For example, if $T_1, T_4,$ and T_2 are faulted, i_a will be zero whereas both i_b, i_c will lose their positive and negative half-cycles, respectively.

F. Current-Sensor Fault

Detection of current-sensor failure is crucial to avoid derating the drive system due to its involvement in the entire control structure. Under normal conditions, the sum of the measured three currents equals zero. However, any deviation from this condition indicates the occurrence of either a current-sensor fault or a ground fault [33]. Given that the fault occurs in phase a (i_a is continuously set to zero due to sensor fault), while the state of the remaining phase currents is unchanged for an open-loop control aspect. The measured three line currents can be formulated as

$$\begin{cases} i'_a = |i'_a| = 0 \\ i'_b = I_m\sin(\omega t - \frac{2\pi}{3}) \\ i'_c = I_m\sin(\omega t + \frac{2\pi}{3}) \end{cases} \tag{13}$$

$$i'_a + i'_b + i'_c = I_m\sin(\omega t + \pi) \neq 0. \tag{14}$$

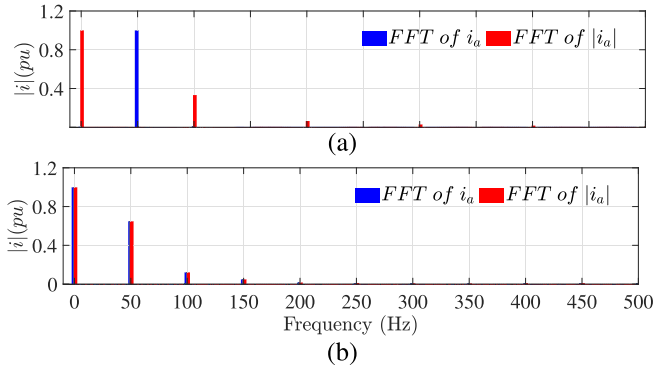

Fig. 2. FFT of motor line current and its absolute component. (a) Healthy case. (b) Faulty case (open switch in phase a).

III. Proposed Fault Diagnosis Scheme

The proposed method leverages the dc components of both line currents and their absolute components associated with fault occurrence, as discussed in the previous section, to detect various fault types. Fig. 2(a) depicts a fast Fourier transform (FFT) of the motor line current i_a and its absolute component $|i_a|$ during the system operation under the healthy case.

As depicted, the line current i_a employs only the fundamental component while the dc component is zero. On the contrary, the absolute value of the line current $|i_a|$ possesses a nonzero dc component along with a second-order frequency component. Consequently, the ratio between the dc components of i_a and $|i_a|$ will be zero during the healthy conditions. Likewise, Fig. 2(b) shows the FFT of i_a and $|i_a|$ but during T_4 open switch. As seen, i_a and $|i_a|$ exhibit identical content of dc and second-order frequency components. In the case of a lower open switch, the line current as well as its absolute component are equal. As a result, the ratio between their dc components will be $+1$. On the other hand, for an upper open switch, the line current and its absolute are negatively related. Therefore, the ratio between the dc components of the line current and its equivalent absolute will be -1. To extract the dc components, the line current and its absolute are filtered out using DRFs tuned at the fundamental as well as the second-order harmonics as given by (15) and (16). Besides, it is proposed to assign the ratios $i_{abc\text{-ratios}}$ defined by (21) for effective diagnosis of different open-switch cases.

It should be noted that, in cases of open-leg fault as well as faulty current-sensor scenarios, the aforementioned ratio will not help in the detection as it will result in undefined value. However, these fault cases can be primarily detected-based only on the absolute component as its value will be zero. To avoid singularities in the case of open-leg and current-sensor faults, as their detection primarily relies on the absolute component. It should be mentioned that in the case of open-leg fault, the summation of the measured line currents will result in zero. On the other hand, in the case of a faulty sensor, the summation of the measured line currents will be a nonzero value. Therefore, to effectively discriminate open-leg and faulty current sensors, it is suggested to augment the filtered absolute component of the line current summation as per (18). Fig. 3 shows the proposed

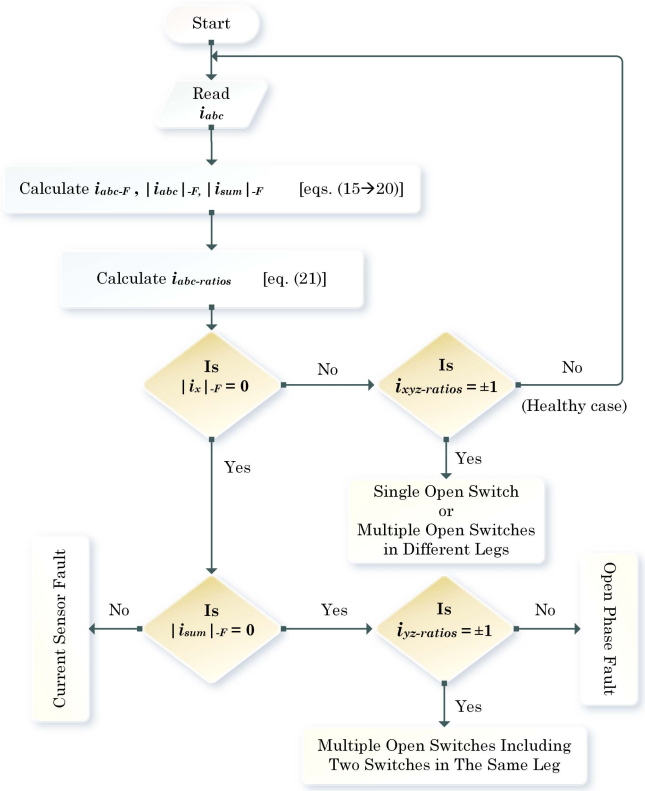

Fig. 3. Flowchart of the proposed fault detection method.

method structure for diagnosis different cases of open-switch and current-sensor faults using the aforementioned variables indicating faults

$$[i_{abc-F}] = [i_{abc}]\,(1 - F_{\omega_1} - F_{2\omega_1})\left(\frac{\omega_c}{s+\omega_c}\right) \tag{15}$$

$$[|i_{abc}|_{-F}] = [|i_{abc}|]\,(1 - F_{\omega_1} - F_{2\omega_1})\left(\frac{\omega_c}{s+\omega_c}\right) \tag{16}$$

$$i_{\text{sum}} = i_a + i_b + i_c \tag{17}$$

$$[|i_{\text{sum}}|_{-F}] = [|i_{\text{sum}}|]\,(1 - F_{\omega_1} - F_{2\omega_1})\left(\frac{\omega_c}{s+\omega_c}\right) \tag{18}$$

$$F_{\omega_1} = \frac{k_f\ {\omega_1}^2\ s}{s^2 + k_f\ {\omega_1}^2\ s + {\omega_1}^2} \tag{19}$$

$$F_{2\omega_1} = \frac{k_f\ (2\omega_1)^2\ s}{s^2 + k_f\ (2\omega_1)^2\ s + (2\omega_1)^2} \tag{20}$$

$$i_{abc\text{-ratios}} = \frac{i_{abc-F}}{|i_{abc}|_{-F}}. \tag{21}$$

IV. Proposed Fuzzy-Based Fault Case Identification

Based on the analysis given in the previous section, a fuzzy-based model is introduced for the final reporting of fault cases. In addition, to ascertain real-time detection, the fuzzy system enables acceleration of fault reporting against the oscillations

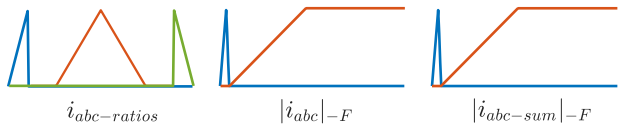

Fig. 4. Fuzzy membership functions.

TABLE I
Summary of Fuzzy-Based Fault Indicators of 33 Fault Scenarios

Case	$i_{a-\text{ratio}}$	$i_{b-\text{ratio}}$	$i_{c-\text{ratio}}$	$\|i_a\|_{-F}$	$\|i_b\|_{-F}$	$\|i_c\|_{-F}$	$\|i_{\text{sum}}\|_{-F}$
Healthy	Z	Z	Z	NZ	NZ	NZ	Z
Single open switch							
T_1	N1	Z	Z	P	—	—	Z
T_4	P1	Z	Z	P	—	—	Z
T_3	Z	N1	Z	—	P	—	Z
T_6	Z	P1	Z	—	P	—	Z
T_5	Z	Z	N1	—	—	P	Z
T_2	Z	Z	P1	—	—	P	Z
Multiple open switches							
T_1, T_6	N1	P1	Z	—	—	P	—
T_3, T_4	P1	N1	Z	—	—	P	—
T_1, T_2	N1	Z	P1	—	P	—	—
T_5, T_4	P1	Z	N1	—	P	—	—
T_5, T_6	Z	P1	N1	P	—	—	—
T_3, T_2	Z	N1	P1	P	—	—	—
$T_1, T_3, (T_2)$	N1	N1	P1	P	P	—	—
$T_4, T_6, (T_5)$	P1	P1	N1	P	P	—	—
$T_1, T_5, (T_6)$	N1	P1	N1	P	—	P	—
$T_4, T_2, (T_3)$	P1	N1	P1	P	—	P	—
$T_3, T_5, (T_4)$	P1	N1	N1	—	P	P	—
$T_6, T_2, (T_1)$	N1	P1	P1	—	P	P	—
T_1, T_4	—	—	—	Z	P	P	Z
T_3, T_6	—	—	—	P	Z	P	Z
T_5, T_2	—	—	—	P	P	Z	Z
$T_1, T_4, (T_3 \mid T_2)$	—	N1	P1	Z	P	P	Z
$T_1, T_4, (T_5 \mid T_6)$	—	P1	N1	Z	P	P	Z
$T_3, T_6, (T_1 \mid T_2)$	N1	—	P1	P	Z	P	Z
$T_3, T_6, (T_5 \mid T_4)$	P1	—	N1	P	Z	P	Z
$T_5, T_2, (T_1 \mid T_6)$	N1	P1	—	P	P	Z	Z
$T_5, T_2, (T_3 \mid T_4)$	P1	N1	—	P	P	Z	Z
Faulty sensor							
S_a	—	—	—	Z	P	P	P
S_b	—	—	—	P	Z	P	P
S_c	—	—	—	P	P	Z	P
S_a, S_b	—	—	—	Z	Z	P	P
S_b, S_c	—	—	—	P	Z	P	P
S_c, S_a	—	—	—	Z	P	Z	P

$T_k, T_l, (T_m)$ means that T_m may or may not be open.
$T_k, T_l, (T_m \mid T_n)$ means that either one or both of T_m and T_n are open.

of the extracted fundamental dc components caused by the employed DRF around the steady-state value. This can be realized by implementing predefined fuzzy membership limits. The identification of faulty switches or current sensors can be determined utilizing three main indicators, i.e., $|i|_{-F}$, i_{ratio} for each phase, and $|i_{\text{sum}}|_{-F}$. Accordingly, seven variables are selected as inputs to the proposed fuzzy subsystem to determine the specific fault type. The entire system, including both inputs and outputs, is defined through the application of fuzzy set theory. During the fuzzification process, the numerical input data are defined as follows: i_{ratio} input of each phase are characterized as negative one (N1), zero (Z), and positive one (P1). Similarly, $|i|_{-F}$ for each phase and $|i_{\text{sum}}|_{-F}$ input variables are categorized using two linguistic variables: zero (Z) and positive (P). Ranges of the input variables, as well as their represented memberships, are formulated by (22), (23), and Fig. 4, respectively. The inputs are utilized to identify 33 fault classes according to the rules described in Table I.

TABLE II
IMs PARAMETERS

Parameter	Symbol	Value			Unit
		IM-I	IM-II	IM-III	
Nominal power	P_n	3	3	37	kW
Nominal L–L voltage	V_{LL}	400	415	400	V
Nominal frequency	f	50	50	50	Hz
Number of pole pairs	P	2	2	2	
Stator leakage inductance	L_{ls}	10.3	13	0.724	mH
Stator resistance	r_s	2.34	4.21	0.08233	Ω
Rotor leakage inductance	L_{lr}	10.3	19	0.724	mH
Rotor resistance	r_r	1.7	1.05	0.0503	Ω
Magnetizing inductance	L_m	345	200	27.11	mH
Lumped friction constant	B	0.0068	0.003	0.09	N·m·s
Lumped inertia constant	H	0.0588	0.065	1	N·m·s^2

Following the fuzzification process, numerical crisp values of 0 and 1 are selected to discriminate between healthy and faulty cases. It is worth mentioning that degree of memberships given by (22) and (23) are selected using extensive real-time simulation as well as experimental test cases in order to avoid false detection due to transient oscillations

$$i_{abc\text{-ratio}} = \begin{cases} P1 & 0.95 < i_{abc\text{-ratio}} < 1.3 \\ Z & -0.65 < i_{abc\text{-ratio}} < 0.65 \\ N1 & -1.3 < i_{abc\text{-ratio}} < -0.95 \end{cases} \tag{22}$$

$$|i|_{-F} = \begin{cases} Z & -0.4 \leq |i|_{-F} \leq 0.4 \\ P & |i|_{-F} > 0.4. \end{cases} \tag{23}$$

V. SIMULATION RESULTS

The described system depicted in Fig. 1 with the proposed fault diagnosis scheme is simulated using MATLAB/Simulink. To reveal the efficacy of the proposed scheme, three different motors, two of 3 kW (IM-I, IM-II) and one of 37 kW rating (IM-III) powered by two-level VSI with parameters specified in Table II are studied during variety of open-switch fault cases.

A. Impact of Loading on the Proposed Method

To prove the efficacy of the proposed scheme and its independence of load ratio, T_1 open-switch fault is carried out during no-load and full-load scenarios for IM-I, as shown in Figs. 5 and 6, respectively. At the onset of loading, the change in the fault detection signals $i_{abc\text{-ratios}}$ is negligible and, therefore, avoids malfunctioning, as shown in Fig. 6(c) at $t = 1s$. In addition, the value of $i_{abc\text{-ratios}}$ remains around zero at normal operation. On the other hand, when the open-switch fault occurs at $t = 2s$ in both cases, the relevant detection signals change markedly, thus, the fault can be easily discriminated from the other normal transient cases.

B. Single Open Switch

Fig. 7(a) demonstrates diagnosis approach behavior in response to T_1 open switch for IM-I during full-load. As depicted, prefault, the ratio $i_{a\text{-ratio}} = i_{a-F}/|i_a|_{-F}$ is zero indicating healthy situation. In contrast, post-fault at $t = 2s$, i_{a-F} is turned negative while its corresponding $|i_a|_{-F}$ remains positive.

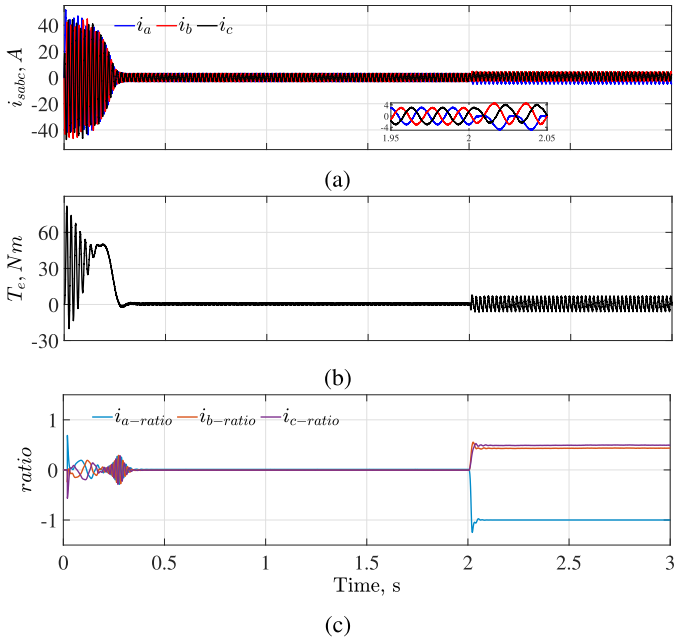

Fig. 5. IM-I output signals due to open switch T_1 during no load. (a) Stator currents. (b) Motor torque. (c) $i_{abc\text{-ratios}}$.

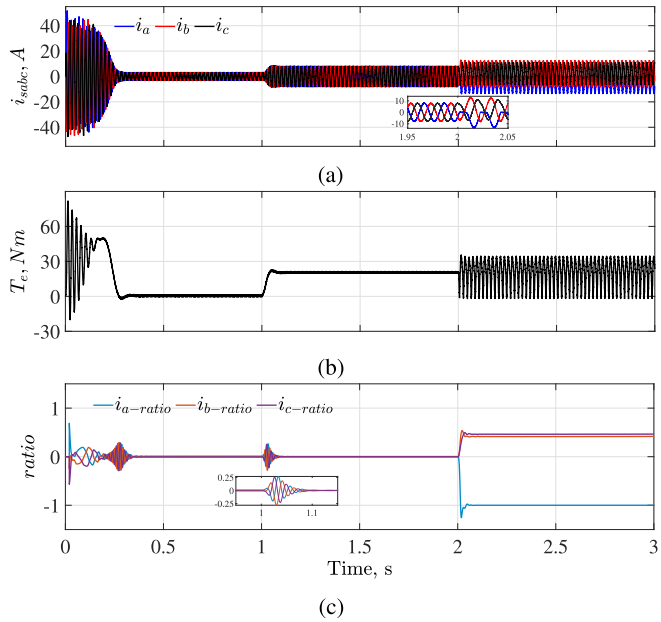

Fig. 6. IM-I output signals due to open switch T_1 during full load. (a) Stator currents. (b) Motor torque. (c) $i_{abc\text{-ratios}}$.

It is noteworthy that $i_{a-F} = -|i_a|_{-F}$, hence, their ratio $i_{a\text{-ratio}}$ is -1 standing for T_1 open-switch fault case, which conforms to the analysis given in Section III.

Similarly, results during fault in the lower switch at the same leg (i.e., T_4) are presented in Fig. 7(b). Unlike the upper switch T_1 fault, the value of i_{a-F} is attained at a positive level during the fault period and the ratio $i_{a\text{-ratio}}$ is $+1$. Although the other ratios $i_{b\text{-ratio}}$, $i_{c\text{-ratio}}$ changed in response to the faults, their values are maintained away from the defined fault level, i.e., ± 1 as described in Section III.

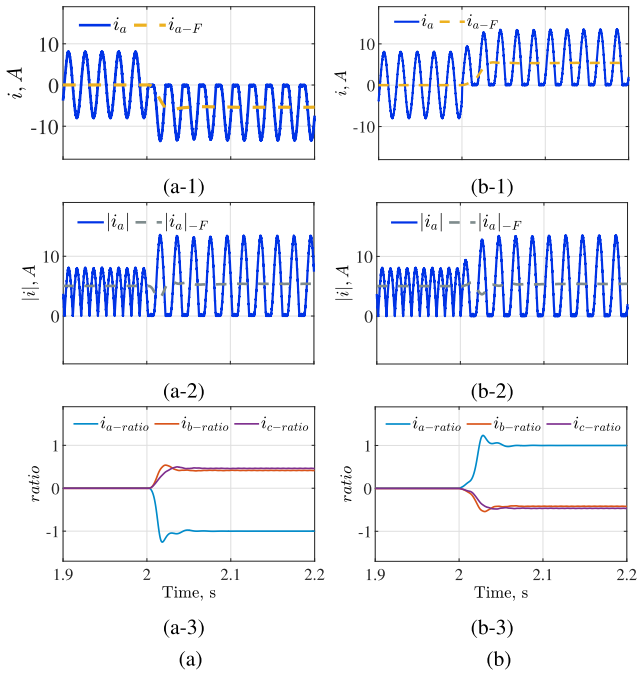

Fig. 7. Output results for IM-I during full load: (a) Open switch T_1. (b) Open switch T_4. (a-1) and (b-1) Phase a current and its DC components. (a-2) and (b-2) Absolute phase a current and its DC components. (a-3) and (b-3) $i_{abc\text{-ratios}}$.

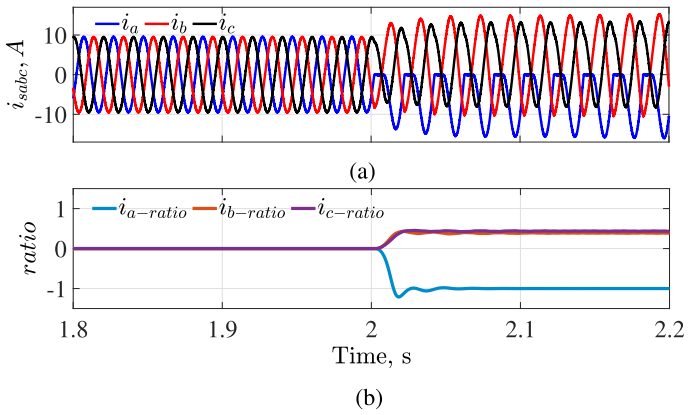

Fig. 8. Output signals due to T_1 open switch during full load for 3 kw IM-II. (a) Stator currents. (b) $i_{abc\text{-ratios}}$.

Another 3 kW IM with different parameters is further tested to validate the independence of the proposed approach on the motor parameters. Fig. 8 shows i_{abc} and $i_{abc\text{-ratios}}$ under T_1 open-switch fault for IM-II. Likewise the case with IM-I (see Fig. 5), post-fault, $i_{a\text{-ratios}}$ reaches a value of -1.

C. Double Open-Switch Fault in Different Leg, Upper and Lower Switches

To explore the independence of the proposed algorithm on the motor rating and proper functioning without any modifications, the proposed scheme is applied to 37 kW IM-III. The response of the proposed algorithm during two simultaneous open switches T_1, T_2 for both IM-I and IM-III is illustrated in Fig. 9. In response to this fault type, $i_{a\text{-ratio}}$, $i_{c\text{-ratio}}$ change to -1, $+1$, respectively,

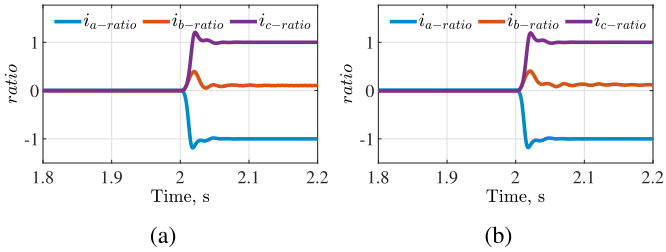

Fig. 9. Output results due to open switches T_1 and T_2 during full load for different rating motors. (a) IM-I. (b) IM-III.

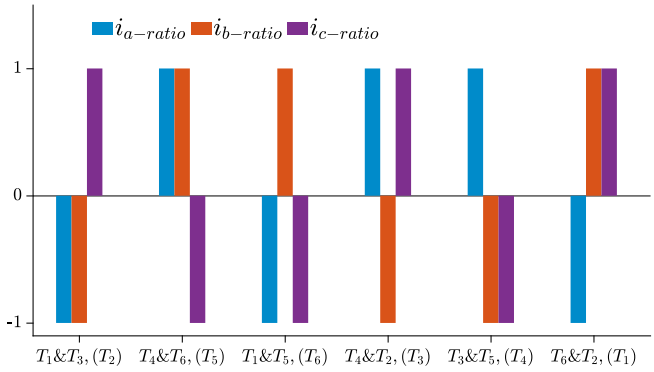

Fig. 10. Summary for the three currents ratios ($i_{abc\text{-ratios}}$) during two open switches both upper or lower.

as described in Table I. In addition, the proposed algorithm performs similarly regardless of the motor capacity.

D. Double Open-Switch Faults, Both Upper or Lower

This scenario involves two open-switch faults in different legs with both switches positioned either upper or lower as demonstrated in Fig. 10.

In this fault type, when two switches are instantaneously faulted, a third switch correspondingly becomes open circuit even if it is healthy as previously discussed in Section II-C due to cease of current flow in an open circuit. If the two open switches are upper, the ratios of their respective phases will be negative while that of the third phase will be positive. On the contrary, if the two faulted switches are lower positioned, their associated phases' ratios will be positive while the other phase is negative.

E. Open-Leg and Current-Sensor Faults

Open-leg faults entail the presence of two open switches within the same leg, whereas, current-sensor faults may comprise one or two faulty sensors. Results for open-leg as well as current-sensor faults for IM-I are depicted in Fig. 11.

During an open-leg fault, the current of its associated phase becomes zero. Therefore, one of $|i_{abc}|_{-F}$ is zero while the remaining two values of the healthy legs increase significantly compared to normal conditions [see Fig. 11(a)]. Therewith, during open-leg faults, $|i_{\text{sum}}|_{-F}$ is maintained zero. Nevertheless, in the case of faulty sensor, the value of $|i_{\text{sum}}|_{-F}$ is inherently a nonzero positive value, as shown in Fig. 11(b). It is noted that, for open-leg and current-sensor faults, $|i_{abc}|_{-F}$ behave similarly.

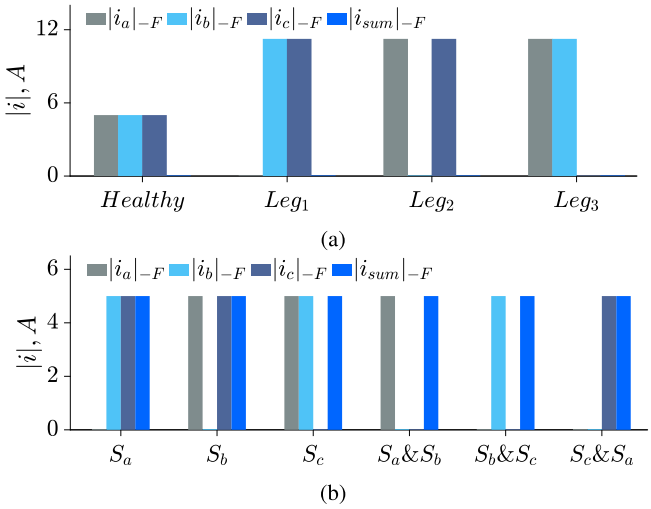

Fig. 11. Graph for filtered absolute currents values $|i_{abc}|_{-F}$ and $|i_{\text{sum}}|_{-F}$ for IM-I during (a) open-leg fault cases and (b) totally broken current-sensor fault cases.

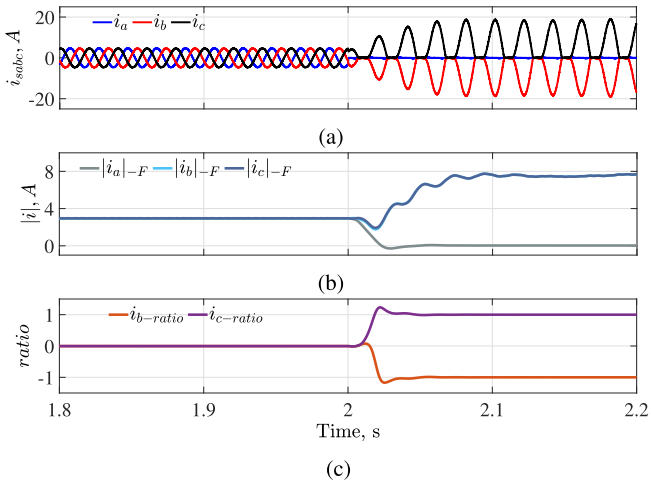

Fig. 12. Output results for IM-I due to open switches T_1 and T_4 and (T_3 or T_2) during half load. (a) Stator currents. (b) $|i_{abc}|_{-F}$. (c) $i_{bc\text{-ratios}}$.

However, in favor of employing $|i_{\text{sum}}|_{-F}$ along with $|i_{abc}|_{-F}$, these two fault types can be discriminated effectively.

F. Three Open-Switch Faults Including Open Leg

In this test, three switches are intentionally opened, with two of them located within the same leg of the circuit. Fig. 12 illustrates the IM-I current and the relevant detection signals during three open switches, T_1, T_4, and T_3 while the motor operates at its half-load. In response to this fault, the switch T_2 loses its conduction period as it depends on the conduction of T_1 and T_3. Therefore, the $|i_a|_{-F}$ ratio is decreased to zero indicating that the first leg is opened. In addition, both $i_{b\text{-ratio}}$ and $i_{c\text{-ratio}}$ change to -1 and $+1$. It means both T_2 and T_3 lose their conduction as described in Section II-E. Notably, the same behavior yields if T_1, T_4, and T_2 are faulted as the conduction of T_3 depends on T_2, T_4.

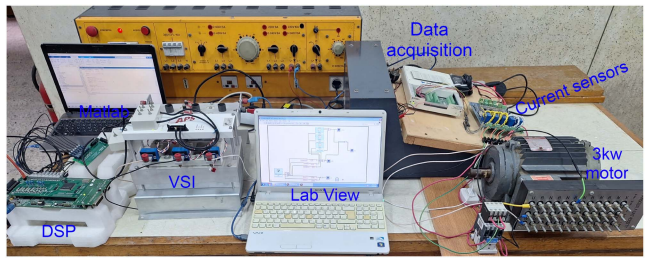

Fig. 13. Experimental setup.

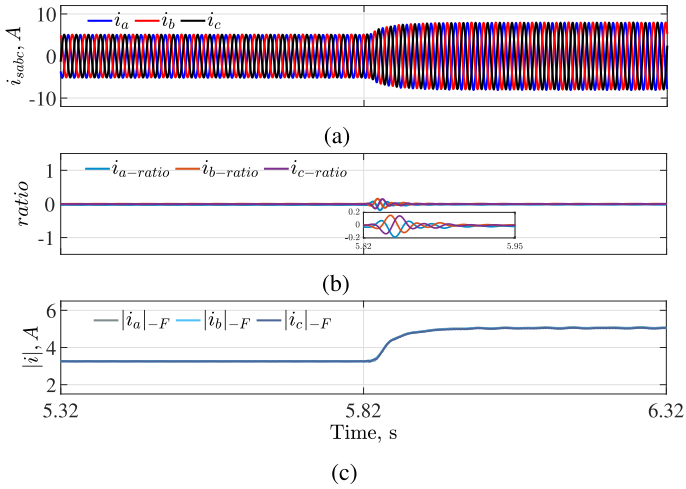

Fig. 14. Experimental results during sudden change in load. (a) Stator currents. (b) $i_{abc\text{-ratios}}$. (c) $|i_{abc}|_{-F}$.

VI. Experimental Results

To further verify the effectiveness of the proposed algorithm, an experimental setup is conducted based on a 3 kW three-phase IM fed by a two-level VSI, as shown in Fig. 13. A control algorithm as well as the proposed fault detection scheme are digitized and performed utilizing a Texas Instruments TMS320C6713 DSP along with an Actel FPGA A3P400-based boards and host port interface (HPI) daughter card. LEM LA 100-P current transducers along with LabView-based data acquisition board are used to capture the motor currents for offline data analysis. In addition, the identified fault detection signals are detected online through MATLAB subroutine associated with the HPI.

A. Sudden Change in Load Effect

Fig. 14 illustrates the effect of sudden change in load on the behaviors of $i_{abc\text{-ratios}}$ and $|i_{abc}|_{-F}$. The machine is loaded with two parallel dc generators, and a sudden load is applied at $t \simeq 5.82s$. Although the pivotal fault indicators $i_{abc\text{-ratios}}$ and $|i_{abc}|_{-F}$ encountered transient changes at the loading moment, they do not indicate for fault incidence.

B. Fuzzy Model Implementation

During the experimental validation, the motor voltage is set to be at 70% of its rated value keeping the ratio V/f constant and the switching frequency is set to 10 kHz. Five selected open-switch faults are demonstrated here to explore the fuzzy model

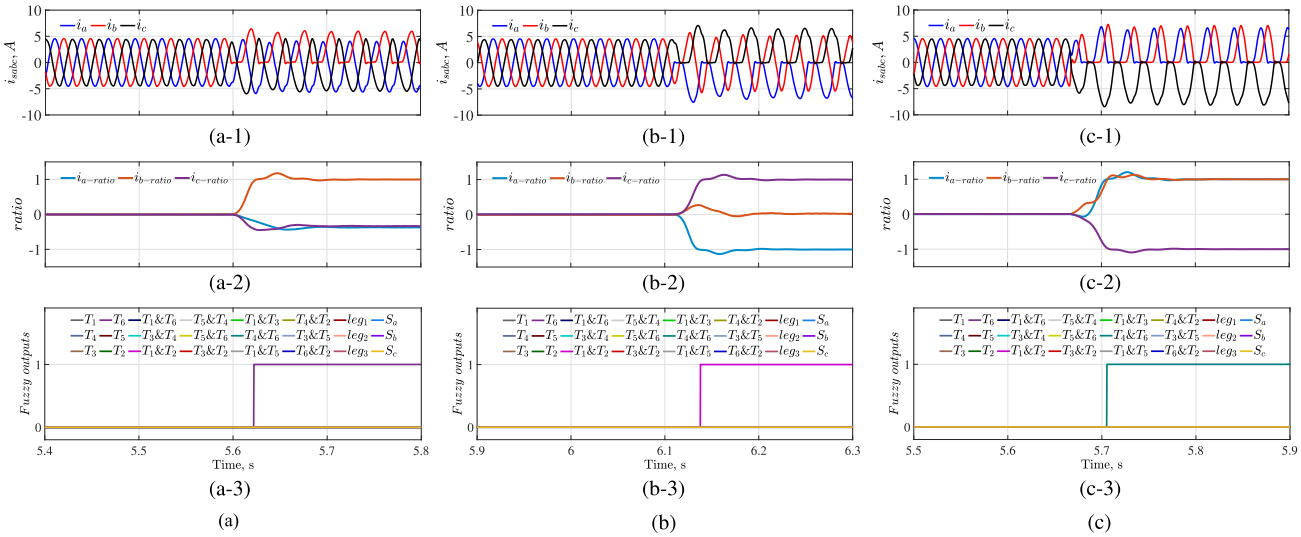

Fig. 15. Experimental results during open-switch faults: (a-1), (b-1), and (c-1) Stator currents. (a-2), (b-2), and (c-2) $i_{abc\text{-ratios}}$. (a-3), (b-3), and (c-3) Fuzzy outputs. (a) Open switch T_6. (b) Open switches T_1 and T_2. (c) Open switches T_4 and T_6.

behavior in response to these faults as previously discussed in Section IV.

Fig. 15(a) presents the three-phase currents, $i_{abc\text{-ratios}}$, and the fuzzy model outputs for T_6 open-switch fault. Post-fault, the $i_{abc\text{-ratios}}$ respond by the rewarded distinctive behavior that is fed to the fuzzy model to decide the fault pattern.

Results for two concurrent open switches in different legs, i.e., T_1 and T_2 (one upper and one lower) are shown in Fig. 15(b). Accordingly, both $i_{a\text{-ratio}}$ and $i_{c\text{-ratio}}$ are attained, i.e., -1, $+1$, respectively, after the fault occurrence, and therefore, the fuzzy output pinpoints this fault. Notably, in the case of two open-switch faults, one current ratio reaches its limit before the other one, and therefore, maloperation as a single open-switch fault may be decided instead. However, when $i_{a\text{-ratio}}$ reaches 0.95, the corresponding value of $i_{c\text{-ratio}}$ exceeds 0.65, representing the threshold for zero membership in the fuzzy model given in (22). This safeguards against the initial misdiagnosis of the T_1 fault fuzzy output, as its rule shown in Table II is not satisfied under these conditions. Generally, during more than open switches in different legs, if one current reaches its limit, the value of the other will be between the center and outer memberships, hence, it will not be identified as a single open-switch fault. Once the two currents reach the specified ratios of -0.95 or $+0.95$, the fuzzy output is initiated identifying the fault case.

Fig. 15(c) shows the experimental results for two lower faulty open switches T_4 and T_6. In this case, both $i_{a\text{-ratio}}$ and $i_{b\text{-ratio}}$ give the rewarded pattern of this fault, i.e., $+1$, while -1 for $i_{c\text{-ratio}}$ as depicted in Fig. 15(c-2). The fuzzy output is activated and a faulty case is identified after the magnitudes of the specified three ratios exceed 0.95.

Fig. 16 illustrates the experimental results for open-leg fault with opening T_3 and T_6. Upon fault occurrence, $|i_b|_{-F}$ decreases to zero whereas $|i_{\text{sum}}|_{-F}$ remains at zero, as shown in Fig. 16(b). Subsequently, the fuzzy output successfully identifies this fault as presented in Fig. 16(c). Moreover, the current-sensor S_a fault is depicted in Fig. 17. In this scenario, the value of

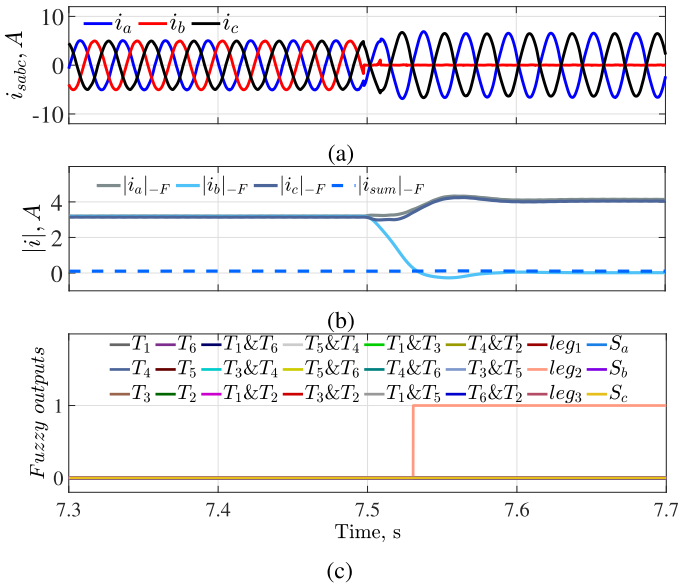

Fig. 16. Experimental results of open leg (T_3 and T_6). (a) Stator currents. (b) $|i|_F$. (c) Fuzzy outputs.

the corresponding current, i.e., $|i_a|_{-F}$ is decreased to zero. In contrast to an open-leg fault, $|i_{\text{sum}}|_{-F}$ increases from zero to a positive value.

C. Effect of Using Two Current Sensors

While three current sensors are typical for high-power inverters, low-power IM drives often function properly with only two current sensors [34]. In this case, the unobserved current can be obtained from

$$i_a + i_b + i_c = 0. \tag{24}$$

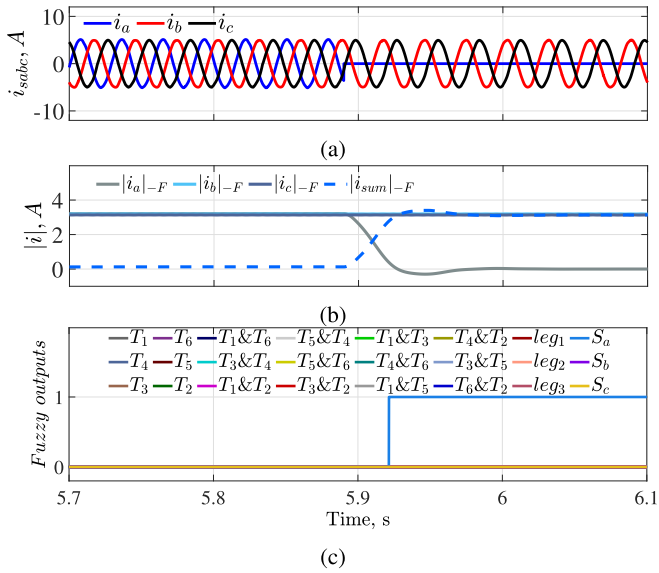

Fig. 17. Experimental signals during faulty sensor S_a. (a) Stator currents. (b) $|i|_F$. (c) fuzzy outputs.

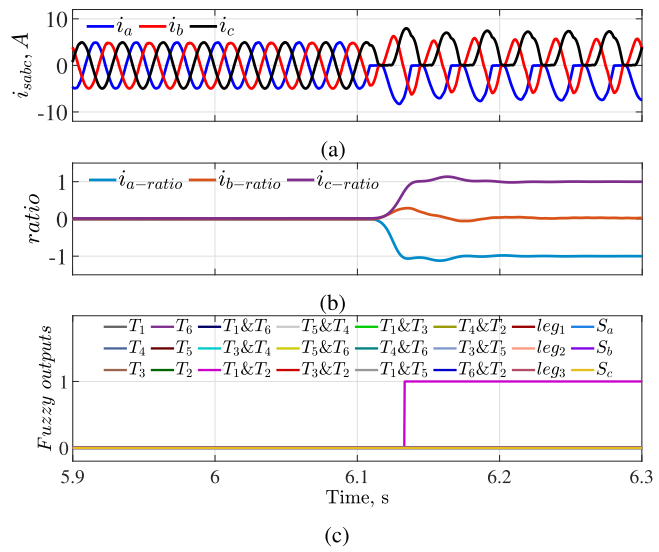

Fig. 18. Experimental results of open switches (T_1 and T_2) using two current sensors. (a) Stator currents. (b) $i_{abc\text{-ratios}}$. (c) Fuzzy outputs.

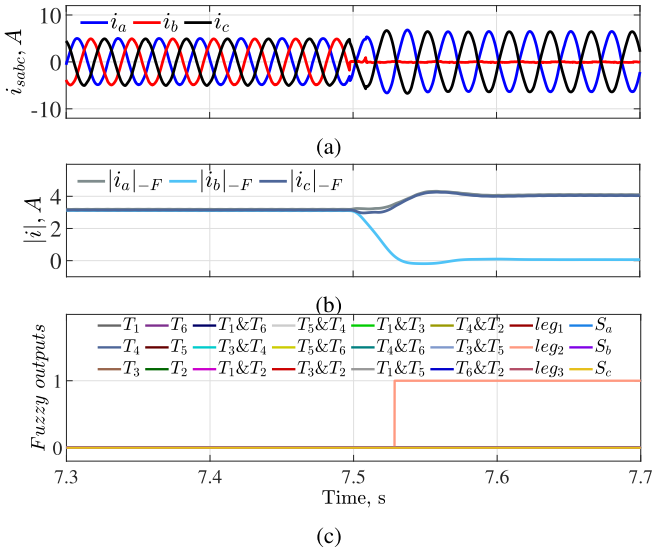

Fig. 19. Experimental results of open leg (T_3 and T_6) using two current sensors. (a) Stator currents. (b) $|i|_F$. (c) Fuzzy outputs.

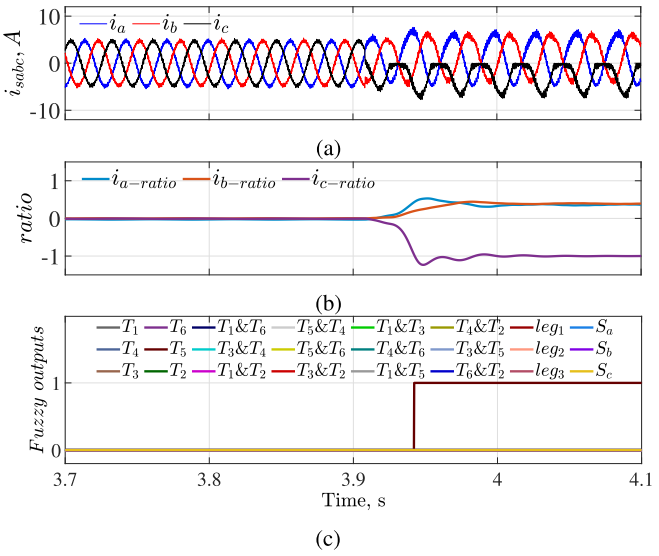

Fig. 20. Experimental results of open switch T_5 during 1 kHz switching frequency. (a) Stator currents. (b) $i_{abc\text{-ratios}}$. (c) Fuzzy outputs.

Assuming that i_a and i_c are measured, while i_b is calculated using (24), an experimental investigation is presented in Figs. 18 and 19 to mimic open-switch faults (T_1, T_2), (T_3, T_6), respectively.

The performance of the detection approach in these cases conforms to that in Figs. 15(b) and 16 with three current-sensors employed. Hence, using two current sensors does not affect the accuracy of detecting open-switch and open-leg faults. However, using $|i_{\text{sum}}|_{-F}$ to discriminate current-sensor fault and an open-leg fault will be ineffective. This is because if a fault occurs in one of the two current sensors, the third current calculated from the previous relationship will be incorrect and the fault will be detected as an open-leg fault. In general, it is difficult to detect current-sensor faults in the case of two current sensors using only current signals. Yet, in this case, current-sensor faults are typically detected using an additional observer or a model to differentiate between open-phase and current-sensor faults.

D. *Effect of Switching Frequency Change*

The lower the switching frequency, the higher the ripples content in the current signals. However, due to the incorporation of low-pass filters specified in (15), (16), and (18), the proposed approach efficiently operates in virtue of reliance on the fundamental component of currents. Figs. 20 and 21 illustrate the fault cases of open switch T_5 and open leg (T_1 and T_4), respectively, using a switching frequency 1 kHz. As depicted, despite the higher ripples content in the current [see Fig. 20(a) and 21(a)], identification of the faults

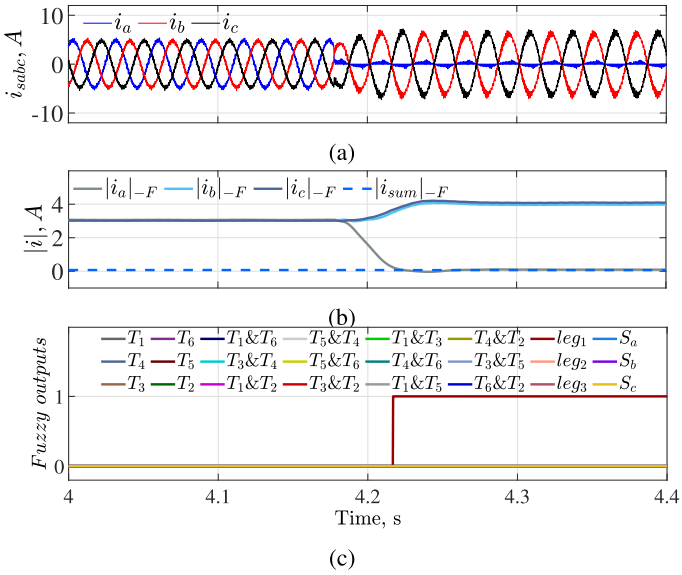

Fig. 21. Experimental results of open leg (T_1 and T_4) during 1 kHz switching frequency. (a) Stator currents. (b) $|i|_F$. (c) Fuzzy outputs.

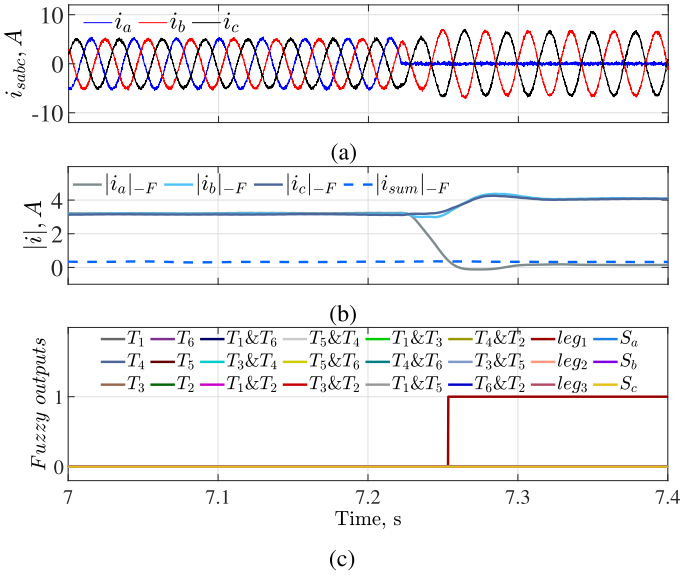

Fig. 22. Experimental results of open leg (T_1 and T_4) in the presence of noise. (a) Stator currents. (b) $|i|_F$. (c) Fuzzy outputs.

is successfully realized as in the case of 10 kHz switching frequency.

E. Effect of Noise Presence

To demonstrate the insensitivity of the proposed method to signal noise, an additive white Gaussian noise with a signal-to-noise ratio of 15 dB is introduced to the current signals, as depicted in Fig. 22.

It is observed that at the fault onset, the value of $|i_a|_{-F}$ dramatically drops close to zero, while $|i_{\text{sum}}|_{-F}$ remains at a value close to zero (as in normal operation), as shown in Fig. 22(b). Consequently, neither of them exceeded the threshold specified in (23) in Section IV.

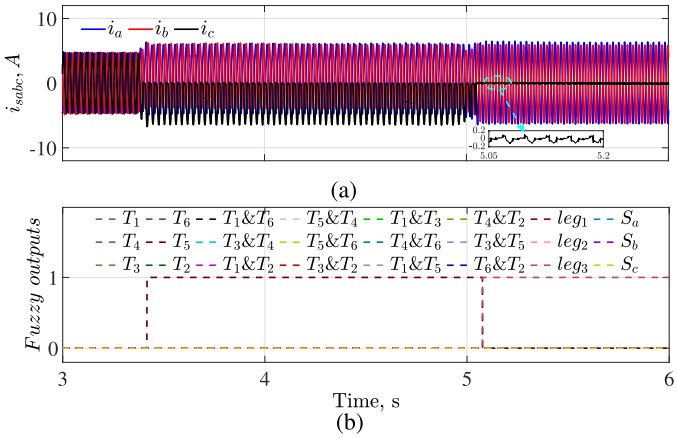

Fig. 23. Experimental results during the sequential opening of T_5 and its associated body-diode D_5. (a) Stator currents, (b) Fuzzy outputs.

F. Comparison With Existing Methods

Table III provides a thorough comparison between the proposed approach and other prominent open-circuit fault diagnosis methods. Key evaluation factors comprising diagnosis capabilities, vulnerability to load variation, noise presence, and switching frequency change. Comparison also incorporates computational complexity, parameter sensitivity, threshold dependence, robustness against false alarms, extra hardware requirements, and detection time, which reveals the significance of the proposed approach.

VII. Limitations of the Proposed Method

Although the proposed method has several merits such as accurate identification of 33 different fault cases. Also, immunity to changes of loading, motor parameters, switching frequency, and noise presence. Nonetheless, discrimination between some cases of two and three open switches (when two switches are in the same positions, either upper or lower) is troublesome due to the resembleness of operational behavior as analyzed in Section II-C. Moreover, it will report the case if one switch and its associated body diode are died as open-leg case. This specific fault case is experimentally investigated in two steps as follows.

First, the firing signals are turned-OFF for T_5, and second, the collector of T_5 is disconnected from the positive dc-link terminal. This resulted in the exclusion of the switch T_5 and its associated body-diode D_5.

As shown in Fig. 23, during the first step, the pulse signal of insulated gate bipolar transistor (IGBT) is removed while its associated body diode is still in operation. The proposed algorithm accurately reported the fault case. On the other hand, when the positive dc link terminal is disconnected from T_5, the diode associated with T_5 is thereby disconnected. Consequently, it blocked the current from flowing through T_2, as T_2 and D_5 are correlated in operation leading to the phase c current and $|i_c|_{-F}$ reaching Zero. Therefore, this specific case gave similar results to the open-leg (T_5 and T_2) fault case. Despite these limitations, to the authors' knowledge, discrimination of the cases above in

TABLE III
COMPARISON WITH EXISTING METHODS

	[18]	[13]	[22]	[31]	proposed method
Method base	Model-based	Voltage-based	Current-based	knowledge-based	Current-based
Diagnosis capabilities	single open switch	single open switch multiple open switches	single open switch multiple open switches open phase	single open switch multiple open switches open phase	single open switch multiple open switches open phase faulty current sensors
Consider load variation	No	Yes	Yes	No	Yes
Consider noise presence	No	No	No	No	Yes
Consider switching frequency change	No	No	No	Yes	Yes
Computational complexity	High	Low	Medium	High	Low
Parameter sensitivity	High	Low	Medium	Low	Low
Dependence of threshold	High	Low	High	-	Low
Robustness against false alarms	Low	Medium	Low	High	High
Extra hardware	No	Yes	No	No	No
Diagnosis time	$0.04:\ 0.167\,T$	T_c (Switching period)	$\sim 2\,T$	$> 2-3\,T$	$0.7-1.25\,T$

motor drive systems is not existed in the motor current-based open-switch fault detection literature. This is due to the high similarity in performance between these cases.

VIII. CONCLUSION

In this article, a novel open-switch fault diagnosis approach for PWM-VSI employing fuzzy logic is presented. The proposed method relies on the measured motor current only, which is filtered and mathematically processed to identify the fault cases. Real-time simulations as well as experimental verification are presented to validate the efficacy of the proposed method. Derived from both simulation analysis along with experimental results, the following conclusions are drawn.

1) The proposed method identifies single and multiple open-switch faults as well as current-sensor faults in VSI-fed IM Drive systems.
2) The proposed method is parameter-less, independent of motor rating or loading effect.
3) The reliability of the proposed method is guaranteed against sudden changes in load, number of utilized current sensors (i.e., two or three), noise presence, and switching frequency change.
4) Fast reporting of faults is ensured which ranges 70% to 125% of the current cycle.
5) The limitation of the proposed method during specific two/three open-switches fault as well as open switch with its associated body diode fault are analyzed and highlighted.

REFERENCES

[1] R. E. K. Meesala and V. K. Thippiripati, "An improved direct torque control of three-level dual inverter fed open-ended winding induction motor drive based on modified look-up table," *IEEE Trans. Power Electron.*, vol. 35, no. 4, pp. 3906–3917, Apr. 2020.

[2] K. Chen, S.-M. Ji, and L. Zhang, "Two-level three-phase voltage source inverter fed low-power AC induction motor based on unipolar pulse-width modulation method," *IET Power Electron.*, vol. 9, no. 3, pp. 435–440, 2016.

[3] M. R. Barusu, U. Sethurajan, and M. Deivasigamani, "Low-cost SPLL-based electrical faults identification for three-phase squirrel cage induction motor using handheld doppler radar signal analysis," *IET Power Electron.*, vol. 11, no. 7, pp. 1205–1216, 2018.

[4] F. W. Fuchs, "Some diagnosis methods for voltage source inverters in variable speed drives with induction machines-a survey," in *Proc. 29th Annu. Conf. IEEE Ind. Electron. Soc.*, 2003, pp. 1378–1385.

[5] F. Wu and J. Zhao, "A real-time multiple open-circuit fault diagnosis method in voltage-source-inverter fed vector controlled drives," *IEEE Trans. Power Electron.*, vol. 31, no. 2, pp. 1425–1437, Feb. 2016.

[6] R. Maamouri, M. Trabelsi, M. Boussak, and F. M'Sahli, "Mixed model-based and signal-based approach for open-switches fault diagnostic in sensorless speed vector controlled induction motor drive using sliding mode observer," *IET Power Electron.*, vol. 12, no. 5, pp. 1149–1159, 2019.

[7] N. Diao, Y. Zhang, X. Sun, C. Song, W. Wang, and H. Zhang, "A real-time open-circuit fault diagnosis method based on hybrid model flux observer for voltage source inverter fed sensorless vector controlled drives," *IEEE Trans. Power Electron.*, vol. 38, no. 2, pp. 2539–2551, Feb. 2023.

[8] C. Yong, J.-J. Zhang, and Z.-Y. Chen, "Current observer-based online open-switch fault diagnosis for voltage-source inverter," *ISA Trans.*, vol. 99, pp. 445–453, 2020.

[9] H. Yin, Y. Chen, and Z. Chen, "Observer-based adaptive threshold diagnosis method for open-switch faults of voltage source inverters," *J. Power Electron.*, vol. 20, pp. 1573–1582, 2020.

[10] B. Wang, X. Feng, T. Sun, Z. Wang, and M. Cheng, "Relative β-axis residual voltage signal based fault detection for inverter switch open-circuit failure," *IEEE Trans. Power Electron.*, vol. 38, no. 9, pp. 11315–11326, Sep. 2023.

[11] R. Manikandan, R. Selvaraj, and R. R. Singh, "Voltage signature based open circuit switch fault diagnosis strategy for IM drives with MPC," *IEEE Trans. Ind. Appl.*, vol. 59, no. 6, pp. 6780–6791, Nov./Dec. 2023.

[12] X. Zhou, Q. Hu, P. Cui, X. Xu, and K. Mao, "A fast open-switch fault and open-winding fault distinguish method based on voltage reference modification," *IEEE Trans. Power Electron.*, vol. 38, no. 9, pp. 11451–11462, Sep. 2023.

[13] M. Trabelsi, M. Boussak, and M. Gossa, "PWM-switching pattern-based diagnosis scheme for single and multiple open-switch damages in VSI-fed induction motor drives," *ISA Trans.*, vol. 51, no. 2, pp. 333–344, 2012.

[14] C. Shu, C. Ya-Ting, Y. Tian-Jian, and W. Xun, "A novel diagnostic technique for open-circuited faults of inverters based on output line-to-line voltage model," *IEEE Trans. Ind. Electron.*, vol. 63, no. 7, pp. 4412–4421, Jul. 2016.

[15] X. Wu et al., "A fast and robust diagnostic method for multiple open-circuit faults of voltage-source inverters through line voltage magnitudes analysis," *IEEE Trans. Power Electron.*, vol. 35, no. 5, pp. 5205–5220, May 2020.

[16] Z. Li, Y. Wang, H. Ma, and L. Hong, "Open-transistor faults diagnosis in voltage-source inverter based on phase voltages with sliding-window counting method," in *Proc. 42nd Annu. Conf. IEEE Ind. Electron. Soc.*. 2016, pp. 435–440.

[17] A. Suti and G. D. Rito, "Diagnosis of power switch faults in three-phase permanent magnet synchronous motors via current-signature technique," *Actuators*, vol. 13, no. 1, 2024, Art. no. 25.

[18] Y. Zhou, J. Zhao, Y. Song, J. Sun, H. Fu, and M. Chu, "A seasonal–trend-decomposition-based voltage-source-inverter open-circuit fault diagnosis method," *IEEE Trans. Power Electron.*, vol. 37, no. 12, pp. 15517–15527, Dec. 2022.

[19] H. Yang, Y. Zhou, and J. Zhao, "Current covariance analysis-based open-circuit fault diagnosis for voltage-source-inverter-fed vector-controlled induction motor drives," *J. Power Electron.*, vol. 20, pp. 492–500, 2020.
[20] N. Raj, J. Mathew, G. Jagadanand, and S. George, "Open-transistor fault detection and diagnosis based on current trajectory in a two-level voltage source inverter," *Procedia Technol.*, vol. 25, pp. 669–675, 2016.
[21] X. Sun, N. Diao, C. Song, Y. Qiu, and X. Zhao, "An open-circuit fault diagnosis method based on adjacent trend line relationship of current vector trajectory for motor drive inverter," *Machines*, vol. 11, no. 10, 2023, Art. no. 928.
[22] H. Yan, Y. Xu, F. Cai, H. Zhang, W. Zhao, and C. Gerada, "PWM-VSI fault diagnosis for a PMSM drive based on the fuzzy logic approach," *IEEE Trans. Power Electron.*, vol. 34, no. 1, pp. 759–768, Jan. 2019.
[23] Y. Yu, J. Hu, Z. Wang, and D. Xu, "IGBT open circuit fault diagnosis in VSI fed induction motor drives based on modified average current method," in *Proc. 9th IEEE Conf. Ind. Electron. Appl.*, 2014, pp. 1334–1338.
[24] Y. Luo, L. Zhang, C. Chen, K. Li, and K. Li, "Real-time diagnosis of open circuit faults in three-phase voltage source inverters," *IEEE Trans. Power Electron.*, vol. 39, no. 6, pp. 7572–7585, Jun. 2024.
[25] W. Wang, Y. Mao, P. Cui, J. Fu, W. Hua, and M. Cheng, "Double normalization fault diagnosis method for open-circuit faults of PMSM drives," *IEEE Trans. Power Electron.*, vol. 39, no. 9, pp. 11613–11624, Sep. 2024.
[26] A. S. Gardouh, A. Ghanem, S. Abulanwar, and E. Gouda, "Current components extraction based open switch fault detection for induction motor drive system," in *Proc. 24th Int. Middle East Power System Conf.*, 2023, pp. 1–8.
[27] A. Ghanem, M. Saeed, S. Abulanwar, W. Hu, F. Deng, and H. Khater, "Padé approximation based open switch fault detection for induction motor drive system," in *Proc. 6th Asia Energy Elect. Eng. Symp.*, 2024, pp. 569–574.
[28] H. Yan, Y. Peng, W. Shang, and D. Kong, "Open-circuit fault diagnosis in voltage source inverter for motor drive by using deep neural network," *Eng. Appl. Artif. Intell.*, 2023, vol. 120, Art. no. 105866.
[29] Y. L. Murphey, M. A. Masrur, Z. Chen, and B. Zhang, "Model-based fault diagnosis in electric drives using machine learning," *IEEE/ASME Trans. Mechatron.*, vol. 11, no. 3, pp. 290–303, Jun. 2006.
[30] H. Xu, Y. Peng, and L. Su, "Research on open circuit fault diagnosis of inverter circuit switching tube based on machine learning algorithm," *IOP Conf. Ser.: Mater. Sci. Eng.*, vol. 452, no. 4, 2018, Art. no. 042015.
[31] Y. Xia and Y. Xu, "A transferrable data-driven method for IGBT open-circuit fault diagnosis in three-phase inverters," *IEEE Trans. Power Electron.*, vol. 36, no. 12, pp. 13478–13488, Dec. 2021.
[32] D. U. Campos-Delgado, J. A. Pecina-Sánchez, D. R. Espinoza-Trejo, and E. R. Arce-Santana, "Diagnosis of open-switch faults in variable speed drives by stator current analysis and pattern recognition," *IET Elect. Power Appl.*, vol. 7, no. 6, pp. 509–522, 2013.
[33] N. M. Freire, J. O. Estima, and A. J. M. Cardoso, "A new approach for current sensor fault diagnosis in PMSG drives for wind energy conversion systems," *IEEE Trans. Ind. Appl.*, vol. 50, no. 2, pp. 1206–1214, Mar./Apr. 2014.
[34] Y. Yu, Y. Zhao, B. Wang, X. Huang, and D. Xu, "Current sensor fault diagnosis and tolerant control for VSI-based induction motor drives," *IEEE Trans. Power Electron.*, vol. 33, no. 5, pp. 4238–4248, May 2018.

Ahmed S. Gardouh was born in Mansoura, Egypt, in 1996. He received the B.Sc. and M.Sc. degrees in electrical engineering from the Faculty of Engineering, Mansoura University, Mansoura, Egypt, in 2019 and 2024, respectively.

His research interests include fault diagnosis of ac motor drive systems, grid-connected converters, AI applications in renewable energy systems.

Sayed Abulanwar (Senior Member, IEEE) received the B.Sc. and M.Sc. degrees in electrical engineering from the Faculty of Engineering, Mansoura University, Mansoura, Egypt, in 2005 and 2010, respectively, and the Ph.D. degree in electrical engineering from Energy Technology Department, Aalborg University, Aalborg, Denmark, in 2016.

He is currently an Associate Professor of Electrical Engineering with the Faculty of Engineering, Mansoura University. He is also with the Faculty of Engineering, Horus University-Egypt, New Damietta City, Egypt. He coauthors the book *AI for Power Electronics and Renewable Energy Systems*. His research includes hybrid ac–dc microgrids, protection of ac and dc systems, intelligent energy systems, transients in power systems, and grid-connected converters.

Dr. Abulanwar is currently an Associate Editor for *IET Renewable Power Generation* and *Alexandria Engineering Journal*. He was a Guest Editor of *IET Renewable Power Generation* for Special Issue: Applications of Artificial Intelligence in Renewable Energy Systems. He was also a Guest Editor for Special Issue: Planning and Operation of Hybrid Renewable Energy Systems, Volume II, *Frontiers in Energy Research*.

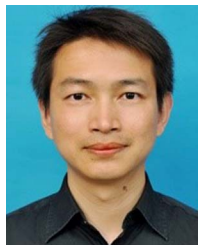

Fujin Deng (Senior Member, IEEE) received the B.Eng. degree in electrical engineering from the China University of Mining and Technology, Jiangsu, China, in 2005, the M.Sc. degree in electrical engineering from Shanghai Jiao Tong University, Shanghai, China, in 2008, and the Ph.D. degree in energy technology from the Department of Energy Technology, Aalborg University, Aalborg, Denmark, in 2012.

From 2013 to 2015 and from 2015 to 2017, he was a Postdoctoral Researcher and an Assistant Professor, respectively, with the Department of Energy Technology, Aalborg University. He joined Southeast University, Nanjing, China, in 2017 as a Professor with the School of Electrical Engineering. His main research interests include wind power generation, multilevel converters, high-voltage direct-current technology, dc grid, and offshore wind farm-power systems dynamics.

Eid Gouda was born in Damietta, Egypt, in 1975. He received the B.Sc. and M.Sc. degrees in electrical engineering from Mansoura University, Mansoura, Egypt, in 1997 and 2004, respectively, and the Ph.D. degree in electrical engineering from the Groupe de Recherche en Électrotechnique et Électronique de Nancy, University Henri Poincare of Nancy, Nancy, France, in 2011.

He is currently a Professor with the Electrical Department, Faculty of Engineering, Mansoura University. His research interests include magnetic gear, electric machine design/control and protection systems, renewable energy, power system analysis, and AI applications in power systems.

Abdelhady Ghanem (Member, IEEE) received the B.Sc., M.Sc., and Ph.D. degrees from Mansoura University, Mansoura, Egypt, in 2006, 2011, and 2017, respectively, all in electrical engineering.

He is currently an Associate Professor of Electrical Engineering with the Faculty of Engineering, Mansoura University. He joined the University of Nottingham, Nottingham, U.K., as an Occasional Ph.D. Student (Joint Supervision Scheme between Mansoura University and University of Nottingham, Nottingham, U.K.) from 2015 to 2017. His research interests include electrical systems modeling, renewable power generation, power system analysis and control, grid-connected power electronics converters, fault diagnosis, and stability analysis.